RIO

PUC

Dissertação de Mestrado

INSIM-NS-3D:

A 3D Numerical Tool for Simulating Waterflooding with Saturation Profile Computed via Numerical Methods

João Pedro Teixeira de Sá

Pontifícia Universidade Católica do Rio de Janeiro
Centro Técnico Científico
Departamento de Matemática

Rio de Janeiro, 25 de setembro de 2025

Pontifícia
Universidade
Católica do
Rio de Janeiro

Dissertação de Mestrado

INSIM-NS-3D:

A 3D Numerical Tool for Simulating Waterflooding with Saturation Profile Computed via Numerical Methods

João Pedro Teixeira de Sá

Orientação: Professor Sinésio Pesco
Coorientação: Professor Abelardo Borges Barreto Jr

Dissertação apresentada como requisito parcial para a obtenção do grau de Mestre em Matemática pelo programa de Pós-Graduação em Matemática, no Departamento de Matemática

Rio de Janeiro, 25 de setembro de 2025

Pontifícia
Universidade
Católica do
Rio de Janeiro

INSIM-NS-3D:

A 3D Numerical Tool for
Simulating Waterflooding with Saturation
Profile Computed via Numerical Methods

João Pedro Teixeira de Sá

Dissertação apresentada como requisito parcial para a obtenção do grau de Mestre em Matemática. Aprovada pela Comissão examinadora abaixo:

Professor Sinésio Pesco
Orientador
Departamento de Matemática – PUC-Rio

Professor Abelardo Borges Barreto Jr
Co-Orientador
Departamento de Matemática – PUC-Rio

Professor José Roberto Pereiro Rodrigues
CENPES - Petrobras

Professor Rodrigo Gusmão Rodrigues
CENPES - Petrobras

Professor Mustafa Onur
Universidade de Tulsa

Rio de Janeiro, 25 de setembro de 2025

Pontifícia
Universidade
Católica do
Rio de Janeiro

João Pedro Teixeira de Sá
Graduou-se em Licenciatura Matemática pela Universidade Federal Fluminense em 2023.

Ficha Catalográfica

Sá, João Pedro Teixeira de
INSIM-NS-3D: A 3D Numerical Tool for Simulating Waterfooding with Saturation Profile Computed via Numerical Methods/ João Pedro Teixeira de Sá; advisor: Sinésio Pesco;co-advisor: Abelardo Borges Barreto Jr. – 2025.

48 f: il. Color. ; 30 cm

Dissertação (mestrado) – Pontifícia Universidade Católica do Rio de Janeiro, Departamento de Matemática, 2025.

Inclui bibliografia

1. Matemática- Teses. 2. Simuladores de fluxo. 3. Engenharia de reservatórios. 4. Modelagem numérica. 5. Injeção de água. 6. Matemática Aplicada. I. Pesco, Sinésio. II. Barreto Junior, Abelardo Borges. III. Pontifícia Universidade Católica do Rio de Janeiro. Departamento de Matemática. IV. Título.

CDD: 510

To my mothers, uncles, aunts, grandparents, sister, and goddaughters.

Acknowledgments

To my advisor, Professor Sinésio Pesco, and Co-advisor, Professor Abelardo Barreto Jr, for encouragement and partnership throughout the development of this work.

This study was financed in part by the Coordenação de Aperfeiçoamento de Pessoal de Nível Superior - Brasil (CAPES) - Finance Code 001.

To FAPERJ, PETROBRAS, and PUC-Rio, for the support provided, without which this work would not have been possible.

This work was made possible only through the partnership with Dimary Moreno, a doctoral student at PUC-Rio.

To Átila Luna and Eduarda Lopes, for giving me the push that led me to pursue graduate studies at PUC-Rio.

To Claudemir and Bruno, fellow graduate students without whom I would never have progressed this far.

To Ana Caroliny, Rômulo B., Clara L., Matheus, and Thais T., great friends from my undergraduate years who were there for me during the most challenging moments of college.

To my mother, for her education, attention, and constant care.

To the professors who served on the examination committee.

To all the professors and staff of the Department of Mathematics, for their teaching and assistance.

To all friends and family who, in one way or another, encouraged or helped me along the way.

Abstract

Sá, João Pedro Teixeira de; Pesco, Sinésio (Advisor); Barreto Junior, Abelardo Borges (Co-Advisor). **INSIM-NS-3D: A 3D Numerical Tool for Simulating Waterflooding with Saturation Profile Computed via Numerical Methods**. Rio de Janeiro, 2025. 47p. Master's thesis – Departamento de Matemática, Pontifícia Universidade Católica do Rio de Janeiro.

The *INSIM-NS-3D* is a proposal for forecasting oil well production under water injection control, based on the *Interwell Numerical Simulation Model with Front-Tracking* (ZHAO et al., 2015) methodology. Despite its applicability in various scenarios, the implementation of *INSIM-FT* has shown limitations, such as mass balance inconsistencies at nodes with multiple connections, difficulties in generalizing to three-phase flow, and high computational cost, mainly due to the saturation calculation using the Front Tracking method. This work proposes a reformulation of the original methodology, aiming to reduce the computational cost associated with saturation transport calculation and, at the same time, solve the observed inconsistencies. The central approach consists of developing numerical solutions for calculating the saturation profile, based on an adaptation of the computational grid. The purpose of this research is to develop a new simulator that seeks to expand the applicability of *INSIM-FT* through numerical solutions for the saturation profile, while maintaining a formulation guided by the physics of flow and respecting the principles of mass conservation. The developed model is designed for two-phase reservoirs, accounting for gravity and compressibility effects.

Keywords

Flow simulation; Reservoir engineering; Numerical modeling; Waterflooding; Apply Mathematics .

Resumo

Sá, João Pedro Teixeira de; Pesco, Sinésio; Barreto Junior, Abelardo Borges . **INSIM-NS-3D: Uma ferramenta numérica 3D para simulação de injeção de água com perfil de saturação calculado por métodos numéricos**. Rio de Janeiro, 2025. 47p. Thesis – Departamento de Matemática, Pontifícia Universidade Católica do Rio de Janeiro.

O *INSIM-NS-3D* é uma proposta de um novo simulador para a previsão da produção de poços de petróleo sob controle por injeção de água, fundamentada na metodologia *Interwell Numerical Simulation Model with Front-Tracking* (ZHAO et al., 2015).Implementações do simulador *INSIM-FT* apresentaram limitações, como inconsistências no balanço de massa em nós com múltiplas conexões, dificuldades de generalização para modelagem de escoamentos trifásicos e elevado custo computacional, principalmente devido ao cálculo da saturação por meio do método *Front Tracking*. Este trabalho propõe uma reformulação da metodologia original, com o objetivo de reduzir o custo computacional associado ao cálculo do transporte de saturação e, simultaneamente, resolver as inconsistências observadas. O simulador desenvolvido neste pesquisa mantem uma formulação orientada pela física do escoamento bifásico e a discretização do reservatório através de caminhos de fluxo e unidades de controle, respeitando os princípios de conservação de massa. O modelo desenvolvido é dirigido a reservatório bifásicos, na presença de gravidade e de compressibilidade.

Palavras-chave

Simuladores de fluxo; Engenharia de reservatórios; Modelagem numérica; Injeção de água; Matemática Aplicada.

Table of contents

List of figures

List of algorithms

List of Abreviations

FT – Front Tracking

BHP – Bottom-hole pressure

INSIM – Interwell Numerical Simulation

ES-MDA – Ensemble Smoother with Multiple Data Assimilation.

Virtue and wisdom are sublime things, but if they create pride and a consciousness of separateness from the rest of humanity, they are only the snakes of self reappearing in a finer form.

Helena P.B, *Collected Writings.*

1
Introduction

The structure of a reservoir, its geological and physical properties, is fundamental to effective modeling, production forecasting, and optimization strategies in the oil and gas industry. Traditional commercial simulators, such as CMG(Computer Modeling Group Ltd., 2024) and Eclipse(Schlumberger, 2024), are well-established tools for these purposes. They provide highly detailed and precise results, which are crucial for project evaluations and investment decisions. However, these simulators come with significant drawbacks, including a strong dependence on extensive laboratory data and detailed reservoir geological characterization which in terms of data increases both the time and cost associated with the modeling process.

Towards of these challenges, data-driven models have emerged as a promising alternative (ALGHAREEB; CHRISTOPHER, 2015; ZHAO et al., 2015; RUDY et al., 2017; BRUNTON; KUTZ, 2019; RAISSI; PERDIKARIS; KARNIADAKIS, 2019; XIE et al., 2020; KISSAS et al., 2020; WILLARD et al., 2020). These models leverage a company's or industry's historical data, often without the need for detailed physical and geological inputs. Their primary advantage lies in their ability to significantly reduce computational costs and the reliance on intensive laboratory and geological information. This approach offers a simplified reservoir simulation.

The Interwell Numerical Simulation model (INSIM) is a data-driven model developed to predict and optimize production on a waterflooding reservoir (ZHAO et al., 2015). It discretizes the reservoir in control units and flow paths, following the IMPES methodology (COATS K.H.; HENDERSON, 1967). One of its key advantages is the reduced number of parameters to be solved. The Interwell Numerical Simulation model with Front Tracking in three dimensions (INSIM-FT-3D)(GUO; REYNOLDS, 2019) was developed to improve INSIM. Maintaining a similar process to define the structure of the reservoir and the associated parameters, but applying a new method to solve the saturation profile analytically defined as Front-Tracking. However, researchers in trials to apply this simulator highlighted issues with the highly computational cost and complexity of the solution, especially with the solution for the saturation profile. In response to these challenges, this research aims to develop a new approach that preserves the INSIM model framework, thereby improving the efficiency and applicability of the INSIM-FT-3D model.

In this work, the Interwell Numerical Simulation Model with Numerical

Saturation in Three Dimensions (INSIM-NS-3D) was developed to reduce computational cost and complexity while enhancing the original simulator's capabilities by incorporating fluid compressibility into the saturation profile equation. This new approach focuses on a numerical solution for the saturation profile, implementing a Finite Difference Method (LEVEQUE, 2002) within an adaptive mesh framework, while preserving the original methodology of describing the reservoir through flow paths and control volumes, and pressure solution. In this framework, a new set of nodes—referred to as intermediate nodes—is introduced along each flow path in the mesh. Unlike INSIM-FT-3D, where the saturation equation is discretized on the edges, in INSIM-NS-3D the discretization is performed at the nodes. Although the pressure equation is also calculated at the nodes, it is not discretized on the intermediate nodes. The procedure to determine an optimal number of intermediate nodes for each edge is beyond the scope of this work; the examples of application have intermediate nodes defined based on empirical observations and comparative results.

This work is organized into five chapters. The second chapter presents a bibliographic review of the INSIM-FT-3D methodology and its implementation, including the mesh generation process, the discretization of the pressure equation followed by the saturation profile on the mesh, an analysis of the computational cost related to the saturation phase, and observations from two application cases. The third chapter introduces INSIM-NS-3D, describing the new mesh structure, adaptations to the pressure equation, the numerical solution of the saturation profile. In fourth chapter two applications are presented comparing results of oil productions obtained from INSIM-NS-3D with IMEX (Computer Modeling Group Ltd., 2024). Finally, the last chapter provides conclusions and discusses directions for future work.

2
Literature Review: Methodology and Implementation of INSIM-FT-3D

In this chapter, we describe the simulation implemented in INSIM-FT-3D, specifying the reservoir and system types, your representations, and the development of the system of partial differential equations to solve.

2.1
Introduction

The Interwell Numerical Simulation Model with front-tracking in three Dimensions (INSIM-FT-3D) is a simulator designed for production optimization and predicting oil on waterflooding in a multilayer reservoir, aimed at solving oil–water systems based on a data-driven model. Developed by Guo (GUO; REYNOLDS, 2019) and based on the INSIM simulator (ZHAO et al., 2015), its implementation involves three key components: 1 - the construction of a three-dimensional mesh with a 1D connective flow path that describes the reservoir with reduce computational cost in comparison to full-reservoir grid; 2 - the absence necessity of prior knowledge about the geological and physical components of the reservoir; and 3- the governing equation to saturation profile is solved by a technique called Front Tracking.The formulation of the pressure equation and the saturation equation is derived from Mass Conservation Law and the principles of mass transport in porous media.

In their work, the model implemented accounts for non-vertically perforated wells. A difference arises in the assumptions used to solve each equation. While the pressure equation assumes the effects of gravity, compressibility, and the absence of capillary action, the saturation profile is determined assuming incompressibility. It is considered a hybrid model, as it combines a physically-based initial approximation with data-driven refinements obtained through a history-matching process using ES-MDA(EMERICK; REYNOLDS, 2013).

In this chapter, we present the procedure for constructing the mesh, the formulation, and procedure to solve the system of equations governing pressure and the saturation profile. Finally, a brief discussion of two applications of this model is also presented.

2.2 Procedure to simulate

The implementation of INSIM-FT-3D is presented in the figure 2.1 . First, a network model is defined on the mesh, characterizing the reservoir as a set of 1D connected flow volumes and unit controls. The unit controls represent wells and areas of interest, defined as Imaginary Wells, graphically represented by nodes. The flow paths describe connections between wells, graphically represented by edges. The process to define the nodes and edges included Mitchell's Best Candidate algorithm (MITCHELL, 1987), Delaunay's Triangulation (PREPARATA; SHAMOS, 1985), Graham Scam(GRAHAM, 1972) and few adjustments to prevent some course structures describe by (GUO; REYNOLDS, 2019). During this process the nodes can be displaced in different depth. With the structure of the mesh well-defined, parameters are introduced.

At well positions, a static bulk volume is defined as a constant value. The pore volume associated with each node i, which is a perforation of a well, is also defined, and it varies in time due to rock compressibility. At the edges, pore volume, which depend on time and rock compressibility, and transmissibility. Those parameters are classified as associated parameters. In figure 2.3 an example of a mesh with four nodes and three edges is presented. The blue points represent the nodes, and the circles indicate the associated porous volume.

INSIM-FT-3D also requires a set of parameters to describe the geological and physical components of the reservoir. Those parameters are initially defined as variables and are calculated by a historical adjustment called ES- (EMERICK; REYNOLDS, 2013). After that, they are established as constant values for all subsequent time steps. This process characterizes this model as a data-driven type model, which operates using previous production data of the reservoir with an arbitrarily chosen set of initial parameters, and is repeated until a minimum error is defined.

The simulator operates in two steps for each time step: first, it solves the pressure equation, and then it describes the saturation profile, following the IMPES methodology (COATS K.H.; HENDERSON, 1967). Pressure is obtained by solving a linear system of equations calculated at the main nodes. At the same time step, saturation profiles are computed by solving a partial differential equation in the form of the Buckley-Leverett equation (BUCKLEY; LEVERETT, 1942) and are calculated at the connections in a analytical method called Front-Tracking.

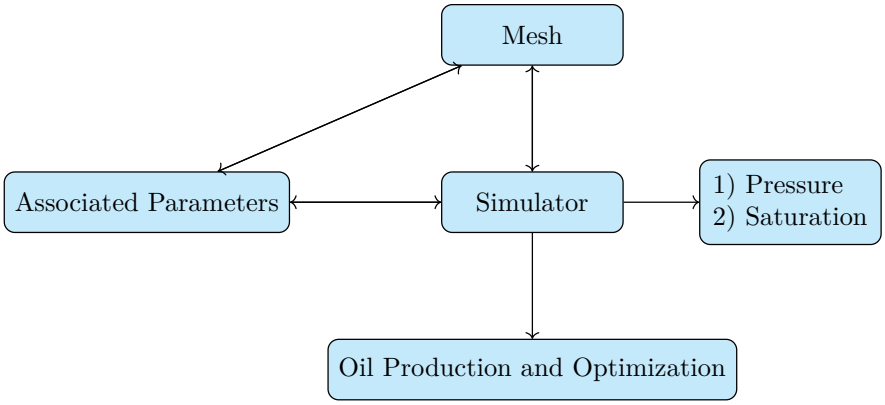

Figure 2.1: Process of INSIM-FT-3D

2.3 Mesh

The reservoir is described as a set of control units and flow paths. The nodes are classified as well perforations or regions of interest in the absence of wells, defined as imaginary wells. The purpose of adding this second category in INSIM-FT-3D, in relation to its predecessor INSIM (ZHAO et al., 2015), is to generate pathways for flow and ensure greater consistency in the results. A simplified example is represented in the figure 2.2 with four nodes. The presence of the imaginary nodes creates two possible flow paths between the nodes associated with a perforation of wells. The procedure to define the number of nodes associated with imaginary wells is based on Mitchell's Best Candidate algorithm (MITCHELL, 1987). A predefined number of points are placed in the mesh using a sample of randomly generated candidates. The point with the highest minimum distance from all previous nodes, including imaginary wells, defines the position of the new imaginary well. This procedure is repeated until the predefined number of imaginary wells is reached. Once establishing all the nodes, including perforation wells and imaginary wells, the next step is to define all the connections.

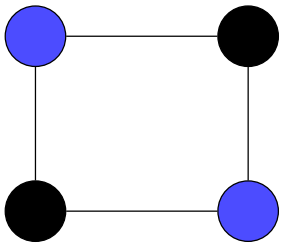

Figure 2.2: Example with four nodes. The blue nodes represent the perforation of wells, while the black nodes represent the imaginary nodes.

With the mesh structure well-defined, it is necessary to establish the

parameters associated with unit controls and flow paths, i.e, nodes and edges. Volumes are associated with the nodes and are described as the porous volume at the nodes. The parameter associated with edges are the transmissibility of the connections and porous volume of the connections. At initial state, the porous volume at the nodes and the transmissibility are defined through history matching using ES-MDA(EMERICK; REYNOLDS, 2013).

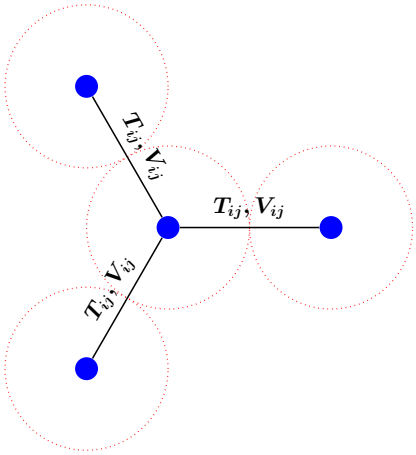

Figure 2.3: Example of mesh with four nodes on INSIM-FT-3D

2.4 Mass Conservation Law

The Mass Conservation Law states that any change in mass within a control volume must be balanced by the net mass flow across its boundaries and by the mass added or removed through sources or sinks (CHEN, 2007). For a two-phase oil water system, this principle leads to the following partial differential equation

$$\underbrace{\frac{\partial(\phi\rho_\alpha S_\alpha)}{\partial t}}_{\text{Accumulation}} + \underbrace{\nabla\cdot(\rho_\alpha\vec{u}_\alpha)}_{\text{Transport}} = \underbrace{\rho_\alpha q_\alpha}_{\text{Source/Sink}} \quad , \quad \alpha = w, o. \tag{2-1}$$

In this equation ϕ is the porosity, ρ_α and S_α are respectively the density and saturation of phase α, $\vec{u}_\alpha$ is its Darcy velocity, and q_α is the volumetric source/sink rate per unit bulk volume at surface conditions. Using Darcy's Law to multiple phases (DARCY, 1856), the velocity $\vec{u}_\alpha$ can be expressed as

$$\vec{u}_\alpha = -\frac{K\,k_{r\alpha}}{\mu_\alpha}\left(\nabla p_\alpha - \rho_\alpha g \nabla z\right). \tag{2-2}$$

The term K represents the absolute permeability tensor of the porous medium, $k_{r\alpha}$ is the relative permeability of phase α, μ_α is the dynamic viscosity

of phase α, p_α is the pressure of phase α, ρ_α is the density of phase α, g is the gravitational acceleration, and z is the depth coordinate. Defining the total mobility as

$$\lambda_t = \lambda_o + \lambda_w, \tag{2-3}$$

where the mobility of phase α is given by the ratio of its relative permeability to its viscosity, namely

$$\lambda_\alpha(S_\alpha) = \frac{k_{r\alpha}(S_\alpha)}{\mu_\alpha}, \qquad \alpha = w, o. \tag{2-4}$$

Neglecting capillary pressure, i.e, considering $p_w = p_o = p$, the mass conservation for the phase α can be described by

$$\frac{\partial(\phi\rho_\alpha S_\alpha)}{\partial t} - \nabla \cdot (K\lambda_\alpha\rho_\alpha(\nabla p - \rho_\alpha g \nabla z)) - \rho_\alpha q_\alpha = 0, \qquad \alpha = o, w. \tag{2-5}$$

The accumulation term can be expanded

$$\frac{\partial(\phi\rho_\alpha S_\alpha)}{\partial t} = \frac{\partial(\phi\rho_\alpha)}{\partial t} S_\alpha + \phi\rho_\alpha \frac{\partial S_\alpha}{\partial t}. \tag{2-6}$$

First term can also be rewrite as

$$\frac{\partial(\phi\rho_\alpha)}{\partial t} = \rho_\alpha \frac{\partial\phi}{\partial t} + \phi \frac{\partial\rho_\alpha}{\partial t}. \tag{2-7}$$

Define rock compressibility c_r and fluid compressibility c_α as

$$c_r = \frac{1}{\phi}\frac{d\phi}{dp}, \quad c_\alpha = \frac{1}{\rho_\alpha}\frac{d\rho_\alpha}{dp}. \tag{2-8}$$

Assuming constant compressibility, the first term of the equation 2-6 can be reduced to

$$\frac{\partial(\phi\rho_\alpha)}{\partial t} S_\alpha = \rho_\alpha \phi S_\alpha (c_r + c_\alpha)\frac{\partial p}{\partial t}. \tag{2-9}$$

Since $S_o = 1 - S_w$, neglecting the spatial variation of ρ_α and adding the

water mass balance equation to the oil mass balance equation we obtain

$$\phi(c_r + S_w c_w + (1 - S_w)c_o)\frac{dp}{dt} - \nabla \cdot (K\left((\lambda_w + \lambda_o)\nabla p - (\lambda_w \gamma_w + \lambda_o \gamma_o)\nabla z\right)) - (q_w + q_o) = 0 \tag{2-10}$$

Defining the total volumetric flow rate q_t as the sum of the phase flow rates. If q_t has a positive value indicates injection and if q_t has negative value indicates production. The total mobility λ_t presented in 2-15 and the compressibility factor c_t, the governing pressure equation is

$$\phi(c_t)\frac{dp}{dt} - \nabla \cdot \left(K\lambda_t \left(\nabla p - \frac{(\lambda_w \gamma_w + \lambda_o \gamma_o)}{\lambda_t}\nabla z\right)\right) - q_t = 0 \tag{2-11}$$

The procedure to apply this equation to the pressure calculation in the mesh is presented in the next subsection. In the following chapters, the variable S will represent the water saturation S_w, and all parameters and equations will follow the International System of Units (SI), in contrast to those presented in (GUO; REYNOLDS, 2019), which uses the Imperial System.

2.5 Pressure System Equation

In INSIM-FT-3D, governing pressure equation is discretized at nodes of the mesh. Following IMPES method (COATS K.H.; HENDERSON, 1967), pressure equation (2-11) is approximated based on the Finite Difference Method (EYMARD; GALLOUËT; HERBIN, 2000). It considers gravitational effects, compressibility and neglect capillarity (see equation (2-11)). The equation for a node i can be described as

$$c_{t,i}^n V_{p,i}^n \frac{\left(p_i^{n+1} - p_i^n\right)}{\Delta t^n} - \sum_{j=n_{0,i}}^{n_{c,i}} T_{ij}^n \left(p_j^{n+1} - p_i^{n+1} + G_{i,j}^n\right) - q_{t,i}^{n+1} = 0 \tag{2-12}$$

where $c_{t,i}^n$ represents compressibility factor and $V_{p,i}^n$ describes the porous volume. The term $n_{k,i}$ represents the nodes connected to node i. An example is presented in figure 2.4.

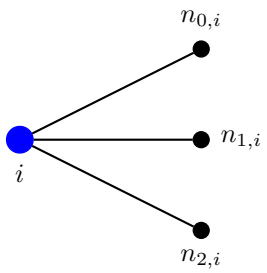

Figure 2.4: An example with main node i connected to three neighbor nodes $n_{0,i}, n_{1,i}, n_{2,i}$.

In INSIM-FT-3D the saturation of the edge between node i and node j, S_{ij}, is calculated by the average between the nodes

$$S_{ij}^n = \frac{1}{2}\left(S_i^n + S_j^n\right). \tag{2-13}$$

The transmissibility of the edge, describe as T_{ij}^n, is defined as

$$T_{ij}^n = \frac{T_{ij}^0}{\lambda_{t,ij}^0}\lambda_{t,ij}^n. \tag{2-14}$$

The transmissibility of the ij at initial state, T_{ij}^0, is assumed a known constant, to be determined by a history-matching procedure, while the total mobility of the edge at initial state, $\lambda_{t,ij}^0$, depends on the initial saturation of the edge S_{ij}^0 . The total mobility of the edge at time t^n for $n > 0$, $\lambda_{t_{ij}}^n$, is calculated as

$$\lambda_{t_{ij}}^n = \lambda_t(S_{ij}^n) = \frac{k_{rw}(S_{ij}^n)}{\mu_w} + \frac{k_{ro}(S_{ij}^n)}{\mu_o}. \tag{2-15}$$

The relative permability of each phase is defined by a Corey type function

$$k_{ro}(S) = (1 - S_{nor})^{n_o}, \tag{2-16}$$

$$k_{rw}(S) = a(S_{nor})^{n_w}, \tag{2-17}$$

where S_{nor} represents the normalized satutarion, given by

$$S_{nor} = \frac{S - S_{iw}}{1 - S_{iw} - S_{or}}, \tag{2-18}$$

in which the irreducible water saturation S_{wi}, the residual oil saturation S_{or} and the power law indices a, n_o, n_w are known constants.

The gravitational term G_{ij}^n is define as

$$G_{ij}^n := \left(\frac{\lambda_w(S_{ij}^n)}{\lambda_t(S_{ij}^n)} \gamma_{w,ij}^n + \frac{\lambda_o(S_{ij}^n)}{\lambda_t(S_{ij}^n)} \gamma_{o,ij}^n \right) (z_i - z_j). \tag{2-19}$$

The depth of node i is represented by z_i, and its defined by the difference of the depth of node and reference depth. The term $\gamma_{\alpha,ij}^n$ represents the specific weight of the phase α at the edge ij and is calculated by the average of the specific weight of the phase of nodes i and j.

$$\gamma_{\alpha,ij}^n = \frac{1}{2} \left(\gamma_{\alpha,i}^n + \gamma_{\alpha,j}^n \right), \qquad \alpha = o, w. \tag{2-20}$$

The specific weight of the phase on the nodes is calculated by

$$\gamma_{\alpha,i}^n = \gamma_{\alpha,i}^0 \left(1 + c_\alpha \left(p_i^n - p^0 \right) \right), \qquad \alpha = o, w. \tag{2-21}$$

The term $\gamma_{\alpha,i}^0$ represents the specific weight of the phase at initial state and p_0 is the reference pressure. Both assumed known constants.

The compressibility factor c_t on node i at time t^n is described as a function of the water saturation

$$c_{t,i}^n = c_t(S_{w,i}^n) = c_r + S_{w,i}^n c_w + \left(1 - S_{w,i}^n \right) c_o. \tag{2-22}$$

The porous volume in node i at time t^n is defined as half of sum of the porous volume for each edge with i as one of extremes

$$V_{p,i}^n = \frac{1}{2} \sum_{j=n_{0,i}}^{n_{c,i}} V_{p,ij}^n. \tag{2-23}$$

The volume of edge ij at time t^n is approximated by a second-order Taylor polynomial as

$$V_{p,ij}^n = V_{p,ij}^0 \left(1 + c_r (p_{ij}^n - p^0) \right). \tag{2-24}$$

The pressure at the edge ij is calculated as the mean of the pressures at the extremes

$$p_{ij}^n = \frac{1}{2}\left(p_i^n + p_j^n\right). \tag{2-25}$$

(GUO; REYNOLDS, 2019) presented the following representation for total well flow rate at a well node i in time t^n for cases where the well is controlled by rate for injection or production. Its definition is based on the Peaceman model (PEACEMAN, 1977) and depends on the difference between the pressure of the node i and the well bottomhole flowing pressure of well $\overline{j}$

$$q_{t,i}^{n+1} = W_{i,\overline{j}}\lambda_{t,i}^n(p_{wf,\overline{j}}^n + H_i^n - p_i^n). \tag{2-26}$$

The term H_i^n accounts for the pressure contribution due to gravity inside the well at node i. It is computed as the sum over all phases of the fractional flow multiplied by the specific weight at surface conditions, multiplied by the vertical depth difference between node i and its associated well reference depth $\overline{j}$:

$$H_i^n = (\gamma_{o,sc}P_{o,i}^n + \gamma_{w,sc}P_{w,i}^n)(z_i - z_{wf,\overline{j}}). \tag{2-27}$$

The fractional contribution of each phase $\alpha \in \{o, w\}$ is given by

$$P_{\alpha,i}^n = \frac{q_{\alpha,i}^n}{q_{t,i}^n}, \qquad \alpha = o, w. \tag{2-28}$$

In nodes associated with imaginary wells, the total flow rate is zero. The Well Index at node i is defined by history match. A similar approach for the total flow is used to define the flow of each phase at node i.

$$q_{\alpha,i}^{n+1} = W_{\overline{j}}\lambda_{\alpha,i}^n(p_{wf,\overline{j}}^n + H_i - p_i^n), \quad \alpha = o, w \tag{2-29}$$

The volumetric total flow of well $\overline{j}$ at time t^{n+1} is described as sum of all total flow rate of each node i associated as a perforation of well $\overline{j}$.

$$q_{t,\overline{j}}^{n+1} = \sum_{i=p_{0,\overline{j}}}^{p_{c,\overline{j}}} q_{t,i}^{n+1}. \tag{2-30}$$

We present below a list of the variables, including their names, metric units use in the equations presented, and whether they are calculated from the history matching process.

List of variables used with units and history match status (SI Units)

Variable	**Description**	**Unit (SI)**	**History Matched?**
$q_{t,i}$	Total flow rate at node i	m^3/s	No
p^0	Initial pressure	Pa	No
W_i	Well Index	$m^3/(Pa \cdot s)$	Yes
ϕ_i	Porosity at node i	–	No
$V_{p,i}$	Pore volume at node i	m^3	Yes
k_i	Absolute permeability at node i	m^2	No
μ_w	Water viscosity	$Pa \cdot s$	No
μ_o	Oil viscosity	$Pa \cdot s$	No
ρ_w	Water density	kg/m^3	No
$c_{t,i}$	Total compressibility at node i	1/Pa	No
T_{ij}^0	Transmissibility between nodes i and j at initial state	$m^3/(Pa \cdot s)$	Yes
$V_{p,\text{tot}}^0$	Total pore volume of the reservoir at time zero	m^3	Yes
a	Coefficient in relative permeability curve	–	Yes
n_o	Oil exponent in relative permeability curve	–	Yes
n_w	Water exponent in relative permeability curve	–	Yes
S_{wi}	Initial water saturation	–	Yes
S_{or}	Residual oil saturation	–	Yes

2.6 Saturation Profile

In INSIM-FT-3D, the saturation profile is solved explicitly at the edge using the equation of mass conservation for water, considering gravitational effects, neglecting capillarity, and assuming incompressibility for the flow. In this section, the partial differential equation describing the transport of water mass will be discretized on the edges of the previously presented mesh. Referring back to equation (2-5), consider the absence of sources or sinks, we obtain

$$\phi\frac{\partial S}{\partial t} - \frac{\partial}{\partial x}\left(K\lambda_w(S)\left(\frac{\partial p}{\partial x} - \gamma_w\frac{\partial z}{\partial x}\right)\right) = 0. \tag{2-31}$$

Considering Darcy's velocity of water as v_w we can rewrite as

$$\phi\frac{\partial S}{\partial t} + \frac{\partial v_w}{\partial x} = 0. \tag{2-32}$$

A dimensionless important function to understand the behavior of the waterflooding reservoir is the fractional flow function of water, f_w, which is defined as the ratio between the velocity of the water and the total Darcy velocity

$$f_w := \frac{v_w}{v_t}. \tag{2-33}$$

Considering the fractional flow and dividing the equation (2-32) for the porosity ϕ, we obtain our equation for the saturation profile.

$$\frac{\partial S}{\partial t} + \frac{v_t}{\phi}\frac{\partial f_w}{\partial x} = 0. \tag{2-34}$$

To discretize this equation on the mesh, we need to define f_w and v_t in terms of the edges. To define water fractional flow, we consider v_t described by pressure and gravity effects for each phase, where we obtain

$$v_t = -K\left[\lambda_w\left(\frac{\partial p}{\partial x} - \gamma_w\frac{\partial z}{\partial x}\right) + \lambda_o\left(\frac{\partial p}{\partial x} - \gamma_o\frac{\partial z}{\partial x}\right)\right]. \tag{2-35}$$

Writing the derivative of the pressure in term of v_t

$$\frac{\partial p}{\partial x} = \frac{-v_t}{K(\lambda_w + \lambda_o)} + \frac{\lambda_w \gamma_w + \lambda_o \gamma_o}{\lambda_w + \lambda_o} \frac{\partial z}{\partial x}, \tag{2-36}$$

and then applying this definition in the description of v_w

$$v_w = \frac{\lambda_w}{\lambda_w + \lambda_o} v_t - K\lambda_w \left(\frac{\lambda_o(\gamma_o - \gamma_w)}{\lambda_w + \lambda_o} \right) \frac{\partial z}{\partial x}, \tag{2-37}$$

the fraction flow function of water can then be described by

$$f_w = \lambda_w \left(\frac{1 - \dfrac{K\lambda_o(\gamma_w - \gamma_o)}{v_t} \dfrac{\partial z}{\partial x}}{\lambda_t} \right). \tag{2-38}$$

This function is defined from $\mathbb{R}^2$ to $\mathbb{R}$, receiving as input the saturation. The output is a value in the interval $[0, 1]$, given by

$$f_w(S_x^t) = \lambda_w(S_x^t) \left(\frac{1 - \dfrac{k_{ij}\lambda_o(S_x^t)(\gamma_{w,ij}^{n-1} - \gamma_{o,ij}^{n-1})}{v_t}(z_i - z_j)}{\lambda_t(S_x^t)} \right) \tag{2-39}$$

with x located on the edge ij and $t^{n-1} \leq t \leq t^n$. The treatment of the edge saturation S_x^t on ij will be discussed further. The total Darcy velocity v_t at edge ij can be approximated by the ratio between the total flow rate $q_{t,ij}$ and the average cross-sectional area A_{ij}.

$$v_t = \frac{q_{t,ij}}{A_{ij}}. \tag{2-40}$$

Solving the linear system of equation for pressure of each node at time step n, we can describe total rate from the edge ij , define by $q_{t,ij}$, as a function of n

$$q_{t,ij}^n = q_{t,ij}(n) = T_{ij}^{n-1} \left(p_j^n - p_i^n + G_{ij}^{n-1} \right). \tag{2-41}$$

A positive value of $q_{t,ij}$ means that the flux on the edge ij goes from node j to node i, while negative means that the flux on the edge ij goes from node i to node j . Rewriting the equation 2-34, discretizing on the edge of the mesh, evaluanting to solve saturation profile at edge ij at time t^n we obtain

$$\frac{\partial S_w(x,\overline{n})}{\partial t}+\frac{q_{t,ij}(\overline{n})}{\phi_{ij}A_{ij}}\frac{\partial f_w(x,\overline{n})}{\partial x}=0 \quad \text{for } 0\leq x\leq L_{i,j}, \quad n-1\leq \overline{n}\leq n. \tag{2-42}$$

The term $q_{t,ij}(\overline{n})$ is assumed equal to $q^n_{t,ij}$ from $n-1$ to n; the average porosity of the edge is describe as ϕ_{ij}; the x represent an position on the edge ij, with $x=0$ equivalent to the position of the node i and $x=L_{ij}$ the position of the node j. The authors suggest that the term $\phi_{ij}A_{ij}$ is not known a priori, so, it can be described by the ration between the pore volume of the edge by the length of the edge

$$\phi_{i,j}A_{i,j}=\frac{V_{p,i,j}}{L_{i,j}}. \tag{2-43}$$

Using (3-43) the equation (3-42) can be rewrite as

$$\frac{\partial S_w(x,\overline{n})}{\partial t}+\frac{q_{t,ij}(\overline{n})L_{ij}}{V^{\overline{n}}_{p,ij}}\frac{\partial f_w(x,\overline{n})}{\partial x}=0 \quad \text{for } 0\leq x\leq L_{i,j}, \quad n-1\leq \overline{n}\leq n. \tag{2-44}$$

The equation that governs the saturation profile is a first-order nonlinear hyperbolic partial differential equation, similar to the Buckley–Leverett formulation:

$$\frac{\partial S}{\partial t}+u\frac{\partial f_w(S)}{\partial x}=0. \tag{2-45}$$

where $S=S(x,t)$.

2.7 Solving a Buckley–Leverett-type Equation

2.7.1 Riemann Problem

The saturation profile of the water phase previous presented is governed by a first-order nonlinear hyperbolic partial differential equation. For each edge ij of the mesh, the problem consists in evaluating $S(x,t)$ for $t > 0$ with initial condition defined by

$$S(x,0) = S^0(x), \tag{2-46}$$

where $S^0(x)$ is the saturation at initial state, given along the edge. This defines a Cauchy problem, and due to the nonlinear nature of $f_w(S)$, when gravity is included in the total velocity v_t, the shape of the graph of $f_w(S)$ may exhibit multiple inflection points. In such cases, standard analytical tools fail to predict the shock structure correctly. To overcome this, the author's (GUO; REYNOLDS, 2019) develop an *convex hull method* in association with a *Front Tracking*, which allows to identify physically admissible solutions.

To apply the convex hull method, we first approximate the original $f_w(S)$ by a piecewise linear curve $\tilde{f}_w$, interpolating the values of f_w at sampled saturations. From this approximation, we construct the convex hull $\text{Conv}(\tilde{f}_w)$ of the graph of $\tilde{f}_w(S)$. The intervals where the convex hull coincides with the original function represent rarefaction waves, while the intervals where the convex hull lies strictly above $\tilde{f}_w$ represent shocks. In the case where the piecewise linear approximation $\tilde{f}_w$ does not contain intervals where the convex hull coincides with $\tilde{f}_w$, the solution consists entirely of shocks, with no rarefaction regions present.

To solve the saturation evolution, the problem on each edge can be locally reduced to several Riemann problems of the form:

$$\frac{\partial S}{\partial t} + v\frac{\partial f_w(S)}{\partial x} = 0, \tag{2-47}$$

with initial condition:

$$S(x,0) = \begin{cases} S_L, & x < x_0, \\ S_R, & x > x_0, \end{cases} \tag{2-48}$$

where S_L and S_R are the left and right saturation states on the edge. The solution of the Riemann problem involves determining whether the transition between S_L and S_R is via a shock, and tracking its position over time.

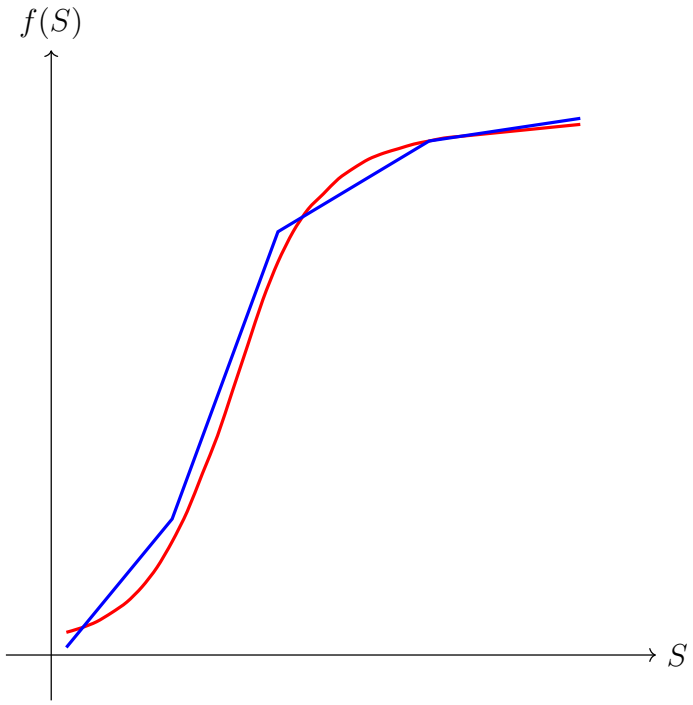

Figure 2.5: The approximation of fractional flow by a piecewise linear function. Adapted from (GRAVE et al., 2024)

In the case of a shock, the discontinuity propagates through the medium at a finite speed σ, given by the Rankine–Hugoniot condition:

$$\sigma = \frac{f_w(S_R) - f_w(S_L)}{S_R - S_L}. \tag{2-49}$$

The admissible solution is given by the convex hull of $\tilde{f}_w(S)$

$$f_w^{\text{admissible}}(S) = \text{Conv}(\tilde{f}_w)(S). \tag{2-50}$$

To compute the solution numerically and track these moving discontinuities explicitly, the authors (GUO; REYNOLDS, 2019) implement a *Front-Tracking method*. To update the position of shock fronts it uses the wave speeds computed from the Rankine–Hugoniot condition. The resulting method is able to solve complex saturation dynamics in the presence of gravity and non-S shape of fractional flow. Fig 2.6 below represents the front-tracking approximation following the Algorithm 11, which describes the Front-Tracking procedure, key-concepts and computational cost of a basic example.

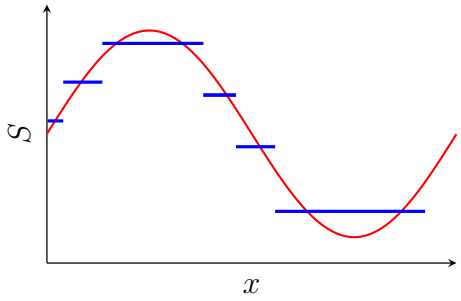

Figure 2.6: A schematic representation of the front-tracking approximations. The approximation of initial conditions by piecewise constant functions. The jumps between consecutive constant segments define the left and right states used to solve the Riemann problems. Adapted from (GRAVE et al., 2024)

Algorithm 1: Front Tracking Algorithm for 1D Saturation Transport

Initial saturation profile $S_w^0(x)$ on $[0, L]$, tolerance ΔS_w, flux function $f_w(S)$ Approximate solution $S_w(x,t)$ at final time

Initialize: Discretize $S_w^0(x)$ into N piecewise constant values: $\{S_{w,i}\}_{i=0}^{N}$

Create initial fronts: for $i = 0$ *to* $N-1$ **do**

$S_{w,i} > S_{w,i+1}$ Shock wave $v \leftarrow \frac{f_w(S_{w,i}) - f_w(S_{w,i+1})}{S_{w,i} - S_{w,i+1}}$ Create shock front at $x_{i+1/2}$ with speed v **else**

Rarefaction wave $M \leftarrow \left\lceil \frac{|S_{w,i+1} - S_{w,i}|}{\Delta S_w} \right\rceil$ **for** $j = 0$ *to* $M-1$ **do**

$S_j \leftarrow S_{w,i} + \frac{j}{M}(S_{w,i+1} - S_{w,i})$ $S_{j+1} \leftarrow S_{w,i} + \frac{j+1}{M}(S_{w,i+1} - S_{w,i})$ $v_j \leftarrow \frac{f_w(S_{j+1}) - f_w(S_j)}{S_{j+1} - S_j}$ Create micro-shock at $x_{i+1/2}$ with speed v_j

Time evolution: for *each time step* $t \to t + \Delta t$ **do**

Move all fronts: $x_{\text{front}} \leftarrow x_{\text{front}} + v_{\text{front}} \cdot \Delta t$

Handle collisions: while *two fronts occupy same position* **do**

Find states S_L and S_R adjacent to the collision Solve Riemann problem for (S_L, S_R) Replace colliding fronts with the new resulting front(s)

Output: Reconstruct $S_w(x,t)$ from final front positions

Key Concepts:

- **Fronts** represent discontinuities in saturation moving with characteristic speeds
- **Shocks** are single fronts moving with Rankine-Hugoniot speed
- **Rarefactions** are approximated by multiple small shocks
- **Collisions** occur when faster fronts catch up to slower ones

Example: For $N = 10$ segments and $\Delta S_w = 0.01$:

- Each shock creates 1 front
- Each rarefaction creates up to $\frac{1.0}{0.01} = 100$ fronts
- Total fronts: potentially $9 \times 100 = 900$
- Each time step: move 900 fronts and check for collisions

Computational Cost Analysis:

- **Front creation:** $\mathcal{O}(N/\Delta S_w)$ operations
- **Collision detection:** $\mathcal{O}(K^2)$ per time step, where K is number of fronts
- **Per time step cost:** $\mathcal{O}(N^2/\Delta S_w^2)$ in worst case
- **Total algorithm complexity:** $\mathcal{O}(T \cdot N^2/\Delta S_w^2)$ for T time steps

Critical bottleneck: The $\mathcal{O}(K^2)$ collision detection dominates computational cost, making the algorithm expensive for small ΔS_w values.

2.8 Observations about the Simulator

Despite the linear system developed for the calculation of pressure and the existence of a weak solution for the Riemann problem, the main issue with the simulation relies on the second phase of the simulator with computational cost, which is significantly high, along with the complexity for applications in three phases or addition of compressibility on the saturation profile.

Besides the cost issue, Li (LI; ONUR, 2023) points to another inconsistency with the INSIM models, including INSIM-FT and INSIM-FT-3D: they do not calculate pressure accurately, even in reservoirs with wells controlled by bottom-hole pressure (BHP). To improve the simulation, they define a new approach that describes the transmissibility along the edges using a harmonic mean and refines the gravity term by considering the partition of saturation along the edges, while maintains the process to pressure equation and saturation profile in INSIM-FT. This new method is called INSIM-BHP.

Following this approach, researchers associated with Petrobras developed a simulator based on INSIM-FT and INSIM-FT-3D to study this issue, as presented in INSIM-BHP (GRAVE et al., 2024). They highlight a mass conservation error in applications of INSIM-FT-3D, especially in meshes with a high number of flow paths connected to the same control unit, but also note a significant reduction of this error when the INSIM-BHP procedure is implemented.

3
INSIM-NS-3D

3.1
Introduction

Interwell Numerical Simulation with Numerical Saturation in three dimensions (INSIM-NS-3D) is a new simulator for oil-water systems in a waterflooding reservoir that relies on a data-driven model. With a similar approach presented by INSIM-FT-3D, in INSIM-NS-3D, the reservoir is described as a set of control units and flow paths represented as nodes and edges.

The nodes are classified into three categories: well perforations, regions of interest in the absence of wells, referred to as imaginary wells, and intermediate nodes. We will refer to the first two types as *original nodes* while the intermediate nodes will be referred to as *new nodes*. While original nodes follow the procedure presented for INSIM-FT-3D, including the definition of the edges, new nodes are placed at the edges. The purpose of adding this new category in INSIM-NS-3D is to develop a numerical solution for the saturation profile using the Finite Volume Method (LEVEQUE, 2002). Our main objectives are to reduce computational cost and complexity in the second phase of the simulator, making it more easily extensible to other problems, such as three-phase flow.

In this chapter, we present the adaptation of the mesh with the inclusion of intermediate nodes, the PDEs governing the pressure equation and saturation profile, and the process of discretizing on this new mesh.

3.2
Mesh

The reservoir is described as a set of control units and flow paths, represented as nodes and edges, following a similar approach that was presented in Section 3.3. The nodes are classified into three categories: well perforations, regions of interest in the absence of wells, and intermediate nodes. This addition is related to the second phase of the simulator: the calculation of the saturation profile, which will be solved numerically using the Finite Volume Method, differently from INSIM-FT-3D, which is discretized only on the nodes. In the following section, the term' original nodes' refers to perforation nodes or imaginary wells, while 'new nodes' refers to intermediate nodes.

The process of defining the position of the original nodes, just as the connection, remains the same as presented earlier, i.e., Mitchell's best candidate algorithm followed Delaunay's Triangulation.

After defining the original nodes and edges, the intermediate nodes are placed on these connections. Several partitions of the edge ij is defined, described as n_{ij}, which establishes the number of new nodes on edge ij. The parameter n_{ij} is chosen based on empirical observation of saturation profile behavior in simulations. The number of new nodes per edge is independent of the number of edges or original nodes.

Figure 3.1 shows an example with three original nodes, i, j, k, and two edges, ij and jk, each with a number of new nodes, given by n_{ij} and n_{jk}, respectively. The distance between two adjacent new nodes in the edge ij is described as ΔL_{ij}. It is calculated as the ratio between the length of the edge and the number of intermediate nodes on the edge plus one.

$$\Delta L_{ij} = \frac{L_{ij}}{n_{ij} + 1} \tag{3-1}$$

The pore volume associated with an intermediate node k_{ij} in the edge ij, described as $V_{p_{k,ij}}$, is defined as the ratio between the pore volume of the edge ij and the number of partitions n_{ij} plus one.

$$V_{p_{k,ij}} = \frac{V_{p_{ij}}}{n_{ij} + 1} \tag{3-2}$$

Recall that the pore volume of the edge $V_{p_{ij}}$ is a parameter calculated by history matching and the pore volume of an original node i in the node mesh is calculated according to Equation (2-24).

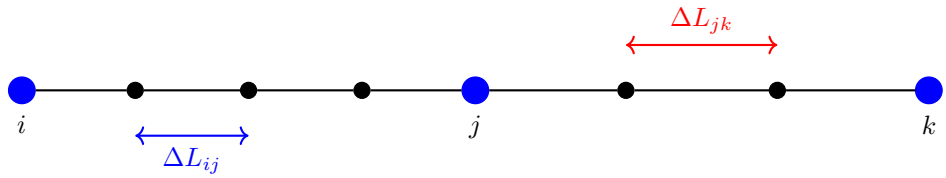

Figure 3.1: Example of mesh with 3 original nodes in blue and 5 intermediate nodes in black.

3.3 Pressure Equation

The pressure equation presented in (2-12), considering the presence of gravity effects, compressibility, and in the absence of capillarity, is discretized on the original nodes of the mesh.

$$V_{p,i}^n c_{t,i}^n \frac{p_i^{n+1} - p_i^n}{\Delta t^n} - \sum_{j=n_{0,i}}^{n_{c,i}} T_{ij}^n \left(p_j^{n+1} - p_i^{n+1} + G_{i,j}^n \right) - q_{t,i}^{n+1} = 0, \tag{3-3}$$

where $n_{k,i}$ represents the k-th element in the set of nodes connected to node i, T_{ij}^n is the transmissibility of the edge, G_{ij}^n is the gravitational factor between the nodes, and $q_{t,i}^n$ is the total rate from node i.

We calculate the transmissibility by

$$T_{ij}^n = \frac{T_{ij}^0}{\lambda_{t,ij}^0} \lambda_{t,ij}^n, \tag{3-4}$$

where $\lambda_{t,ij}$ is the total mobility at the edge ij. Despite pressure being only evaluated at the original nodes, the mobility is calculated by the harmonic mean of all the nodes along the edge, a similar approach presented in (LI; ONUR, 2023),

$$\lambda_{t,ij}^n = \frac{1}{\frac{\Delta L_{ij}}{L_{ij}} \left[\sum_{k=1}^{n_{ij}} \frac{1}{\lambda_t(S_{k,ij}^n)} + \frac{1}{2} \left(\frac{1}{\lambda_t(S_i^n)} + \frac{1}{\lambda_t(S_j^n)} \right) \right]}. \tag{3-5}$$

Here $S_{k,ij}^n$ represents saturation of the k-th intermediate node in the edge ij, and S_i, S_j are the saturations of the nodes i and j. The gravitational term on the edge, described in eq (2-19), is also redefined as the mean of the sum of gravitational terms associated with each intermediate node belonging to the edge, i.e.

$$G_{ij}^n = \sum_{k=1}^{n_{ij}} \left(\frac{\gamma_{w,ij}^n \, \lambda_w(S_{k,ij}^n)}{\lambda_t(S_{k,ij}^n)} + \frac{\gamma_{o,ij}^n \, \lambda_o(S_{k,ij}^n)}{\lambda_t(S_{k,ij}^n)} \right) \cdot \frac{(z_j - z_i)}{n_{ij} + 1}, \tag{3-6}$$

with z_k as the depth of node k and $\gamma_{w,ij}$, $\gamma_{o,ij}$ as the specific weight of water and oil at edge ij, respectively.
with p_0 the pressure of the reservoir at the initial state. With those definitions, the mobility of each phase m associated with the original nodes is calculated by

$$\lambda_{m,i}^n = \frac{k_{rm}(S_i^n)}{\mu_{m,i}^n}. \tag{3-7}$$

Considering only one perforation per well, the total rate at node $q_{t,i}^n$ is a known constant when i is a perforation of well j with control by rate. However, in the case of control by bottom-hole pressure (BHP), the rate is estimated by a Peaceman model(PEACEMAN, 1977):

$$q_{t,i}^n = W_i \lambda_t(S_i^n)(p_{wf,j}^n - p_i^n), \tag{3-8}$$

with well index W_i defined by history matching and total mobility at the node $\lambda_{t,i}$ defined as the sum of mobility of oil and mobility of water as presented in 2-15. The initial saturation at original nodes S_i^0 and at new nodes $S_{k,ij}^0$ is based on the water initial saturation S_{wi}, which is a known constant. The total compressibility is defined by

$$c_{t,i}^n = c_r + c_w S_i^n + c_o(1 - S_i^n). \tag{3-9}$$

3.4 Saturation Profile

In INSIM-NS-3D, the saturation profile is solved at the nodes using the equation of mass conservation of water, considering gravitational effects and compressibility, while neglecting capillarity, under the same conditions as the previous pressure equation. In this section, the partial differential equation that describes the transport of water mass will be discretized at the nodes of the previously presented mesh. Referring back to the equation of mass conservation of water phase (2-5) and following a similar approach presented in INSIM-FT-3D in equation (2-34), we obtain

$$\frac{\partial S}{\partial t} + S(c_r + c_w)\frac{\partial p}{\partial t} + \frac{v_t}{\phi}\frac{\partial f_w}{\partial x} - q_w = 0. \tag{3-10}$$

The dynamics of water saturation profile over time dont follow the time step determined for pressure equation. In saturation profile our time step is defined as intermediate time step between time step t^n and t^{n+1}, $t^{n,p}$, as

$$t^n = t^{n,0}, \tag{3-11}$$

$$t^{n+1} = t^{n,\overline{p}+1}, \tag{3-12}$$

$$t^{n,p} \text{ with } p \in [0, \overline{p}] \tag{3-13}$$

with $\overline{p}$ as the number of intermediate time steps. At first we will discretize only on intermediate nodes at intermediate time steps. Since the pressure is not calculated at intermediate time steps and intermediate nodes, we approximate the pressure at intermediate nodes by interpolating the pressure at the original

nodes of the edge and calculating the derivative for the original time step. For k in the edge ij we approximate pressure by

$$\frac{\partial p}{\partial t} \approx \frac{\overline{k}(p_i^{n+1} - p_i^n) + (1-\overline{k})(p_j^{n+1} - p_j^n)}{\Delta t^n} = \Delta p_k^n. \tag{3-14}$$

The term $\overline{k}$ is the relative position of the intermediate node at the edge and is calculated by the ratio between k and $n_{ij}+1$, which lies in $(0,1)$.

Following the procedure presented previously to define total Darcy's velocity (DARCY, 1856) and implementing the finite difference method (EYMARD; GALLOUËT; HERBIN, 2000), our equation becomes

$$\begin{aligned} V_{p_{k,ij}}^n \left(\frac{S_{k,ij}^{n,p+1} - S_{k,ij}^{n,p}}{\Delta t^{n,p}} + S_{k,ij}^{n,p+1}(c_r + c_w)\Delta p_k^n \right) \\ + q_{t,ij}^{n+1} \left(f\left(S_{k+\frac{1}{2},ij}^{n,\nu}\right) - f\left(S_{k-\frac{1}{2},ij}^{n,\nu}\right) \right) = 0, \end{aligned} \tag{3-15}$$

where ν is defined depending on the treatment chosen. If explicit then $\nu = p$. Otherwise, $\nu = p+1$. The total rate is similar to that presented in equation 2-41, calculated by the pressure associated with the node defined in the previous step, but with inverted orientation:

$$q_{t,ij}^n = -T_{ij}\lambda_{t,ij}\left(p_j^n - p_i^n + G_{ij}^{n-1}\right). \tag{3-16}$$

By discretizing the fractional flow function over the computational mesh and incorporating gravitational effects, we obtain

$$f_{w,ij}(S_{k,ij}^{n,p}) = \frac{\lambda_w(S_{k,ij}^{n,p})}{\lambda_t(S_{k,ij}^{n,p})}\left(1 - \frac{T_{ij}\lambda_o(S_{k,ij}^{n,p})(\gamma_{w,ij}^{n,p} - \gamma_{o,ij}^{n,p})}{q_{t,ij}^n}(z_i - z_j)\right). \tag{3-17}$$

Then we define a piecewise function f for the flux between intermediate node k and node $k+1$ as

$$f\left(S_{k+\frac{1}{2},ij}^{n,\nu}\right) = \begin{cases} f_{w,ij}\left(S_{k,ij}^{n,\nu}\right), & \text{if } p_i^{n+1} \geq p_j^{n+1} + \gamma_{w,ij}^{n+1}(z_j - z_i); \\ f_{w,ij}\left(S_{k+1,ij}^{n,\nu}\right), & \text{if else.} \end{cases} \tag{3-18}$$

and for the flux between intermediate node $k-1$ and k as

$$f\left(S^{n,\nu}_{k-\frac{1}{2},ij}\right) = \begin{cases} f\left(S^{n,\nu}_{k-1,ij}\right), & \text{if } p_i^{n+1} \geq p_j^{n+1} + \gamma^{n+1}_{w,ij}(z_j - z_i); \\ f\left(S^{n,\nu}_{k,ij}\right), & \text{if else.} \end{cases} \tag{3-19}$$

The main difference between the equations for intermediate nodes and original nodes lies in the treatment of fluxes. For original nodes, it is necessary to consider the sum of all incoming and outgoing fluxes at node i. This involves evaluating each edge for which node i is an endpoint and applying upwind weighting to that edge.

$$\begin{aligned} V^n_{p_i}\left(\frac{S_i^{n,p+1} - S_i^{n,p}}{\Delta t^{n,p}} + \frac{(S_i^{n,p+1}(c_r + c_w))(p_i^{n+1} - p_i^n)}{\Delta t^n}\right) \\ + \sum_{j=n_{0,i}}^{n_{c,i}} q^{n+1}_{t,ij}\left(f\left(S^{n,\nu}_{\frac{1}{2},ij}\right)\right) - q^{n+1,\nu}_{w,i} = 0, \end{aligned} \tag{3-20}$$

with $q^{n+1}_{t,ij}$ having a positive sign if the flux goes from node i to node j, and negative sign otherwise. The water rate at node i, $q_{w,i}$, is approximated by the product of the total rate by the ratio between the mobility of water and the total mobility

$$q^{n+1,\nu}_{w,i} = \frac{\lambda_w(S_i^{n,\nu})}{\lambda_t(S_i^{n,\nu})} q^n_{t,ij}. \tag{3-21}$$

The term $S^{n,\nu}_{\frac{1}{2},ij}$ is defined by upstream

$$S^{n,\nu}_{\frac{1}{2},ij} = \begin{cases} S^{n,\nu}_{1,ij}, & \text{if } p_j^{n+1} \geq p_i^{n+1} + \gamma^{n+1}_{w,ij}(z_j - z_i), \\ S_i^{n,\nu}, & \text{otherwise.} \end{cases} \tag{3-22}$$

In the following section, initial results are presented.

4
Results

The INSIM-NS-3D simulator was implemented in Python 3.12, using the most recent stable release available at the time of development (Python Software Foundation, 2024). The programming environment was configured in Visual Studio Code, and the entire project was executed locally. It is important to emphasize that the Python code was designed strictly for academic research purposes. As such, no effort was made to optimize performance, and the implementation does not aim to deliver good—let alone competitive—execution times.

In this chapter, two case studies obtained from source material provided by Petrobras are presented and analyzed. These cases were originally formulated to be evaluated using a C++ implementation of the INSIM-FT-3D model (GUO; REYNOLDS, 2019), developed with a strong focus on numerical optimization and computational efficiency and in absence of compressibility on the saturarion phase. The original INSIM-FT-3D code cannot be used as a baseline for comparison in this work, both because of its optimized nature and because it does not include compressibility effects.

Furthermore, at the time this research was conducted, an INSIM-BHP implementation was not accessible to the research group, making it impossible to perform direct cross-comparison between different INSIM formulations. Therefore, the main objective of the present analysis is to assess the discrepancies between the results produced by the INSIM-NS-3D simulator and those obtained with CMG-IMEX 2024 (Computer Modeling Group Ltd., 2024), with particular attention to total oil production and bottom-hole pressure (BHP).

4.1
Case A: Gravitational effect with two nodes

The first case, referred to as Grav2Nodes, describes a reservoir with two wells with a Datum depth of 2500 meters, represented by seven nodes connected by an inclined edge with a full length of approximately 141.4 meters, and was solved explicit. In this set, two are original nodes, both perforations, and nine are new nodes. The node with represent an perforation of producer well is positioned at coordinates $(x_0, y_0, z_0) = (0\,\text{m}, 0\,\text{m}, 2500\,\text{m})$, while the node which represent an perforation of injector well is located at $(x_1, y_1, z_1) = (100\,\text{m}, 0\,\text{m}, 2600\,\text{m})$. In edge, intermediate nodes are positioned equidistant. An example with two intermediate nodes can be seen in Figure

4.1 below.

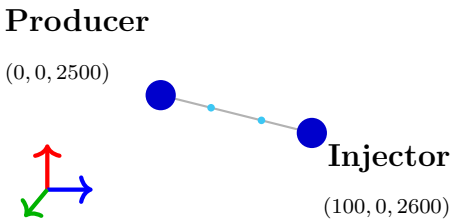

Figure 4.1: Schematic representation of the `Grav2Nodes` mesh, showing an inclined connection between all nodes with perforations of injector and producer wells as the extremes of the edge.

Both wells operate under rate control with $q_t = 10m^3/day$ for the injector and $q_t = 10m^3/day$ for the producer. The total simulation time is 150 days, with a time step of 0.5 hours and an intermediate time step of 0.25 hours. The reservoir has a total pore volume of 1000 m^3 with water initial saturation $S_{wi} = 0$ and residual oil saturation $S_{or} = 0$. Rock, water and oil compressibility are $c_r = 2.17551 \times 10^{-6}(kgf/cm2)$, $c_w = 1 \times 10^{-6}(kgf/cm2)$ and $c_o = 3.57143 \times 10^{-8}(kgf/cm2)$, respectively. Oil density reference is defined as $\gamma_{ref,o} = 715kg/m^3$ and water density as $\gamma_{ref,w} = 1024kg/m^3$. Oil viscosity is $\mu_{ref,o} = 1.0$ cp, and water viscosity is $\mu_{ref,w} = 1.0$ cp. The relative permeability of water and oil are constructed with $k_{rw0} = 0.7$, $n_w = 3.0$ and $n_o = 1.5$, mean permeability $k = 200$ md, porosity of reference $\phi_{ref} = 0.15$. The time of execution registered was 0.661278724 seconds. The data generated included BHP pressure, pressure at the node, water saturation, and oil/water rate at the production well. The original material is in Brazilian System of Units and it is convert in SI during implementation. They can be observed in Figure 4.2.

To reproduce this inclined structure in CMG-IMEX, a grid was created with $10 \times 1 \times 1$ blocks defined with corner-point geometry, inclined in the vertical (Z) direction to represent a sloped structure. The inclination is implemented through the zcorn array, which specifies varying depths for each grid block corner, allowing for accurate representation of dipping layers. Horizontal spacing is uniform with $\Delta x = \Delta y = 10$ m and $\Delta z = 20$ for each block. The x-direction represents the main flow axis, while the vertical variation captures the structural dip of the model. A volume modifier was used to maintain the total pore volume. The grid is represented in the figure 4.3 using Build from CMG.

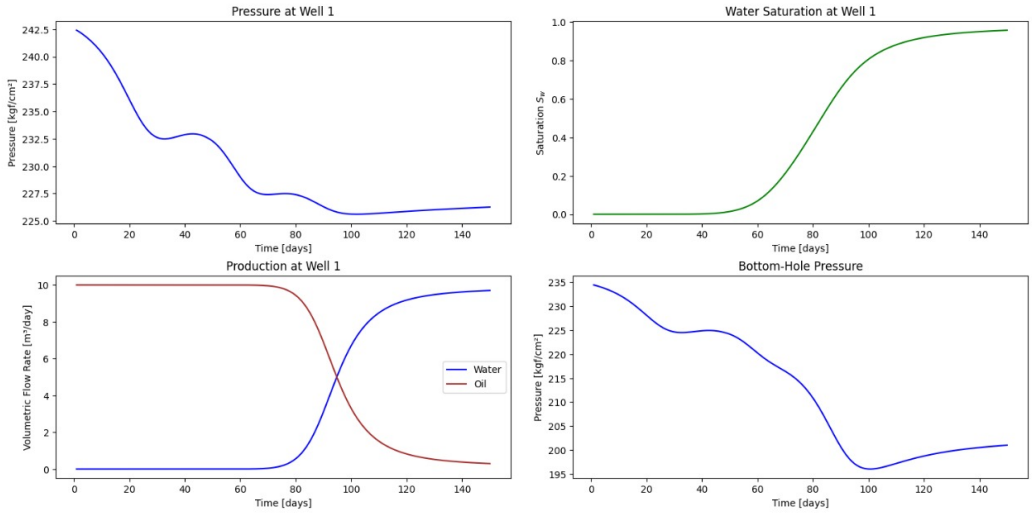

Figure 4.2: Data generated in INSIM-NS-3D for Grav2nodes with two intermediate nodes.

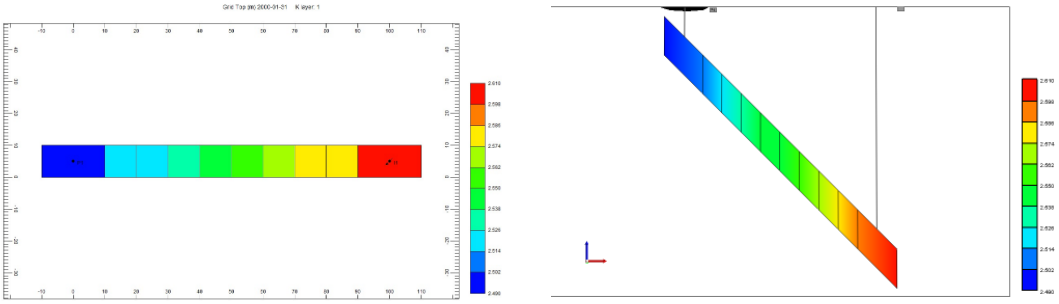

Figure 4.3: Grid in IMEX.

A comparison between the IMEX and INSIM-NS-3D shows an minimal deviation, with total oil production from well P1 differing by 0.13% . The mean difference in oil ate is 0.201512 m^3/day. Tests with two, four, six and eight intermediate nodes were implemented.

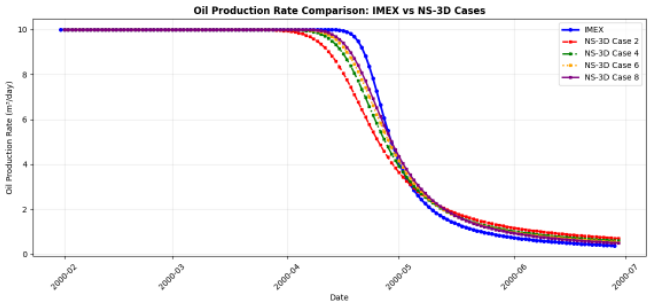

Oil and water production rate comparison (IMEX vs INSIM-NS-3D)

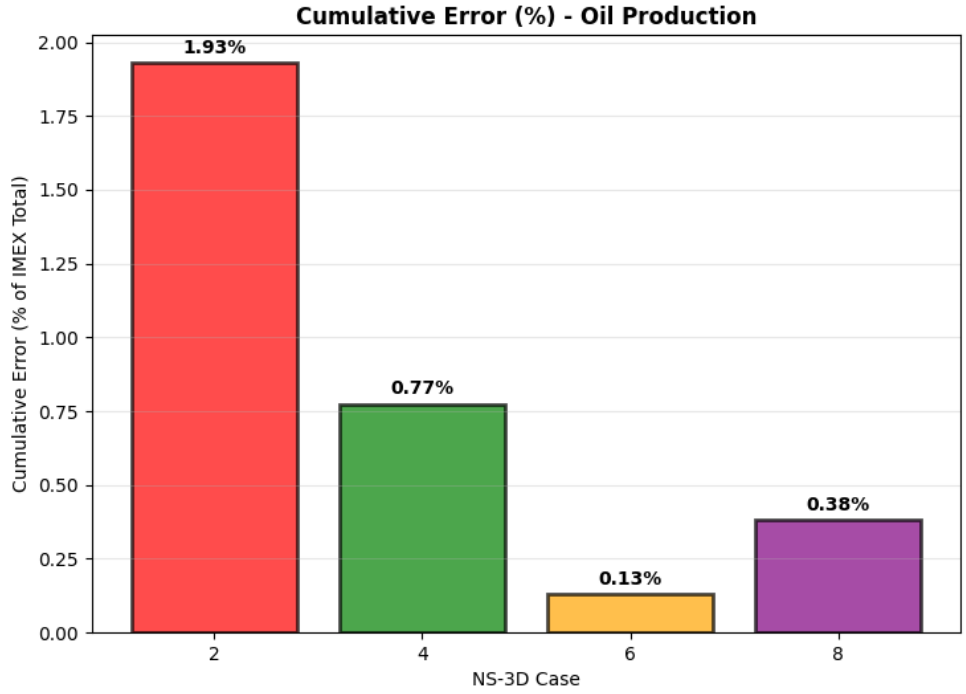

Figure 4.4: Comparison of production rates between IMEX and INSIM-NS-3D in case

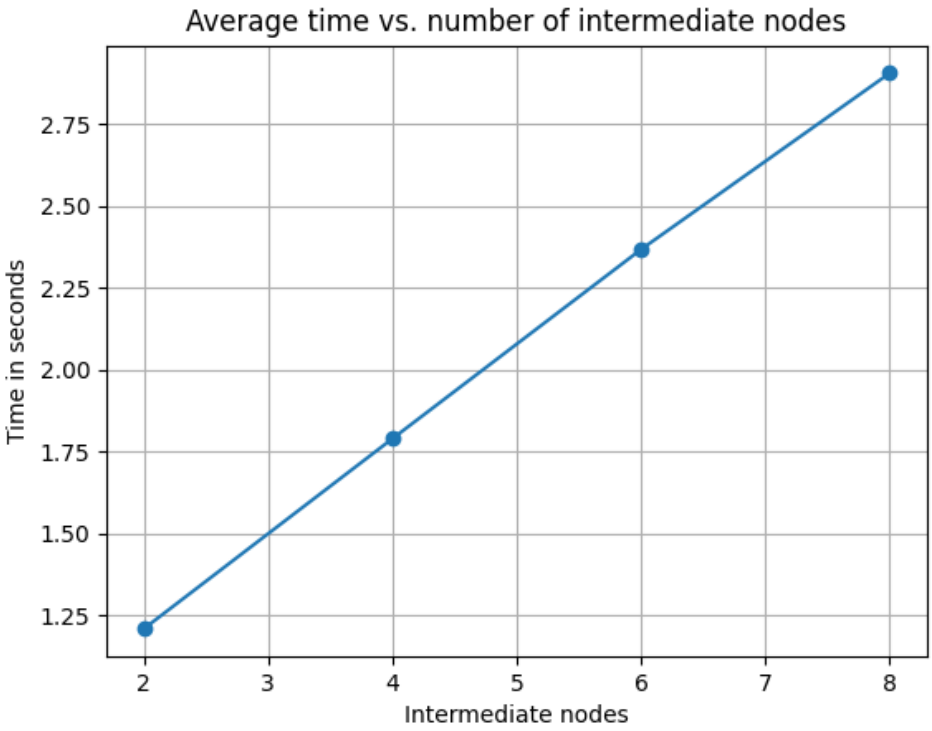

Figure 4.5: Grav2nodes execution time.

4.2 Case B: A Quarter of Five-Spot in a 3D Reservoir

The second case, referred to as Quarter5Spot3D, represents a unit cubic reservoir with an injector and a producer placed at opposite corners. It is a well-known basic test configuration in reservoir simulation, often used to evaluate numerical methods and validate multiphase flow models (CHEN, 2007; KILLOUGH, 1976).

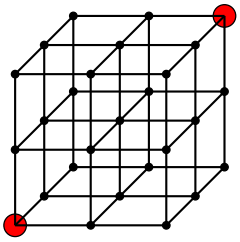

Figure 4.6: Mesh of Quarter5spot3D, where the red dots represent perforations and black dot represent imaginary well.

In this case an reservoir with depth of 2500 meters and with two wells is describe by 27 main nodes, distribute in format of a cube with the mesh and the solved explicity. In this configurations, 2 nodes represent perforations of wells and 25 represent imaginary wells. An visual representation of the reservoir can be seen in figure 4.6 restrict to 27 original nodes. All edges between original nodes have length of 20 meters. The node perforation of injector well is positioned at coordinates $(x_0, y_0, z_0) = (40\,\text{m}, 40\,\text{m}, 2540\,\text{m})$, while the producer well is located at $(x_1, y_1, z_1) = (0\,\text{m}, 0\,\text{m}, 2500\,\text{m})$.

Both wells operate under rate control with $q_t = 100m^3/day$ for injector and $q_t = 100m^3/day$ for productor, the total simulation time is 250 days. Time step implemented of 1 hour and intermediate time step of 0.5 hours. The reservoir has a total pore volume of 5400 m^3 with $S_{wi} = 0$ and residual oil saturation $S_{or} = 0$. Rock, water and oil compressibility are $c_r = 2.17551 \times 10^{-6}(kgf/cm2)$, $c_w = 1 \times 10^{-6}(kgf/cm2)$ and $c_o = 3.57143 \times 10^{-8}(kgf/cm2)$, respectively. Oil density reference is defined as $\gamma_{ref,o} = 715kg/m^3$ and water density as $\gamma_{ref,w} = 1024kg/m^3$. Oil viscosity is $\mu_{ref,o} = 2.373$ cp, and water viscosity is $\mu_{ref,w} = 1.0$ cp. The relative permeability of water and oil are constructed with $k_{rw0} = 0.7$, $n_w = 3.0$ and $n_o = 1.5$, mean permeability $k = 200$ md, porosity of reference $\phi_{ref} = 0.15$. The data generated was BHP pressure, pressure node, water saturation and oil/water rate at the production well in Brazilian System of Units and can be observed on figure 4.2 below.

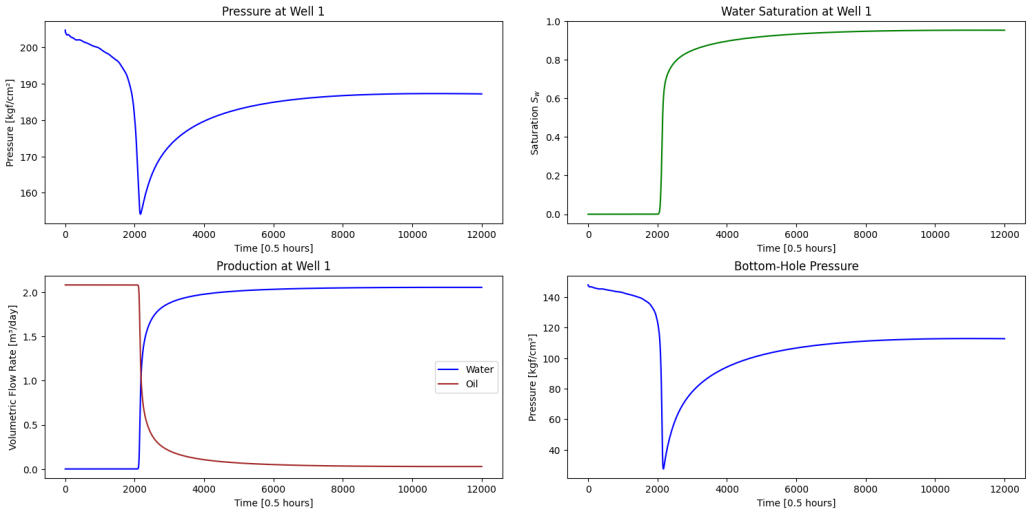

Figure 4.7: Generated data from INSIM-NS-3D in Quarter5spot3D

Comparing the rate production data observed in INSIM-NS-3D with IMEX the difference statistics between the results of oil production corresponds to a relative difference of approximately 2.15%. Tests with two, four, six and eight intermediate nodes were implemented.

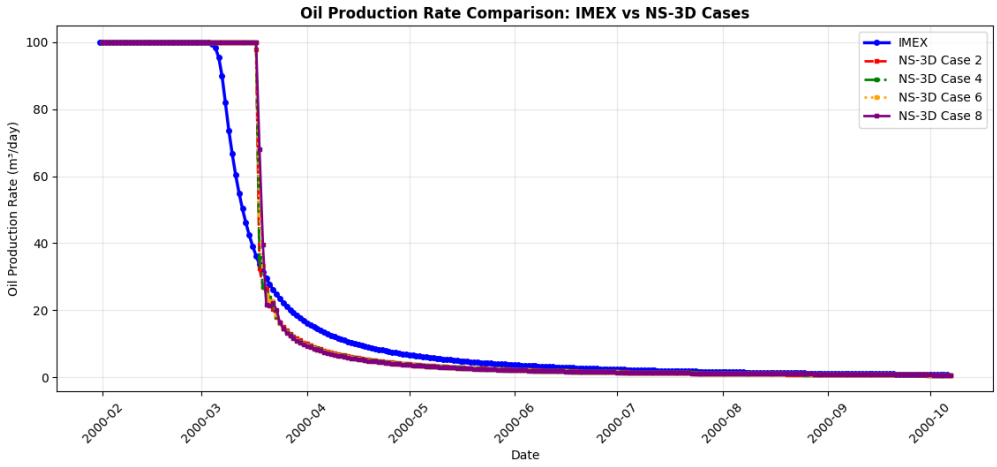

Figure 4.8: Detailed comparison between IMEX and INSIM-NS-3D for Quarter5spot3D

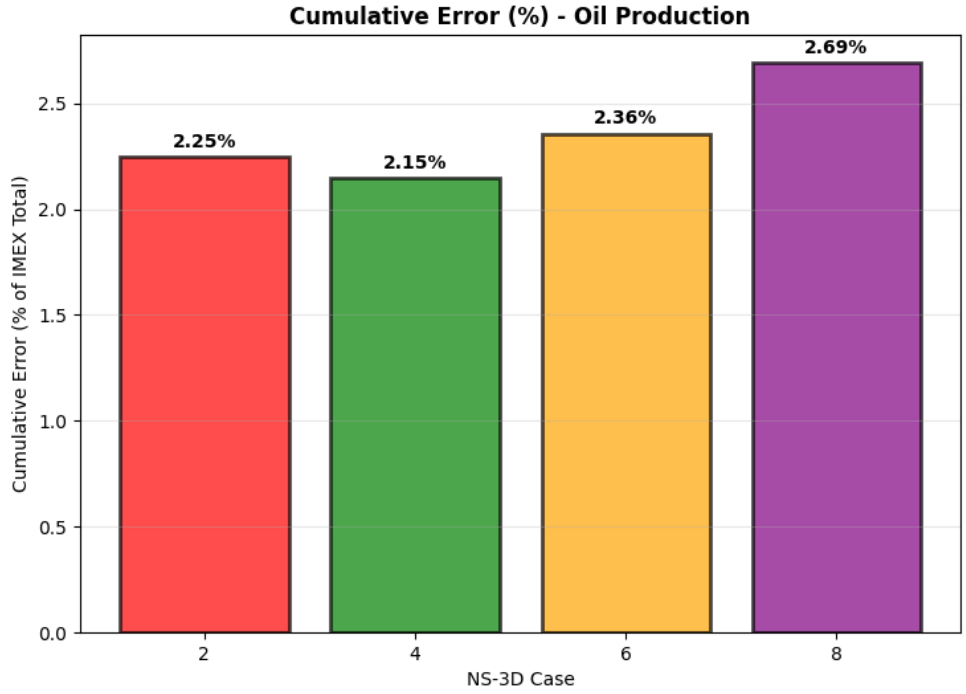

Figure 4.9: Comparison of production rates and execution times between IMEX and INSIM-NS-3D

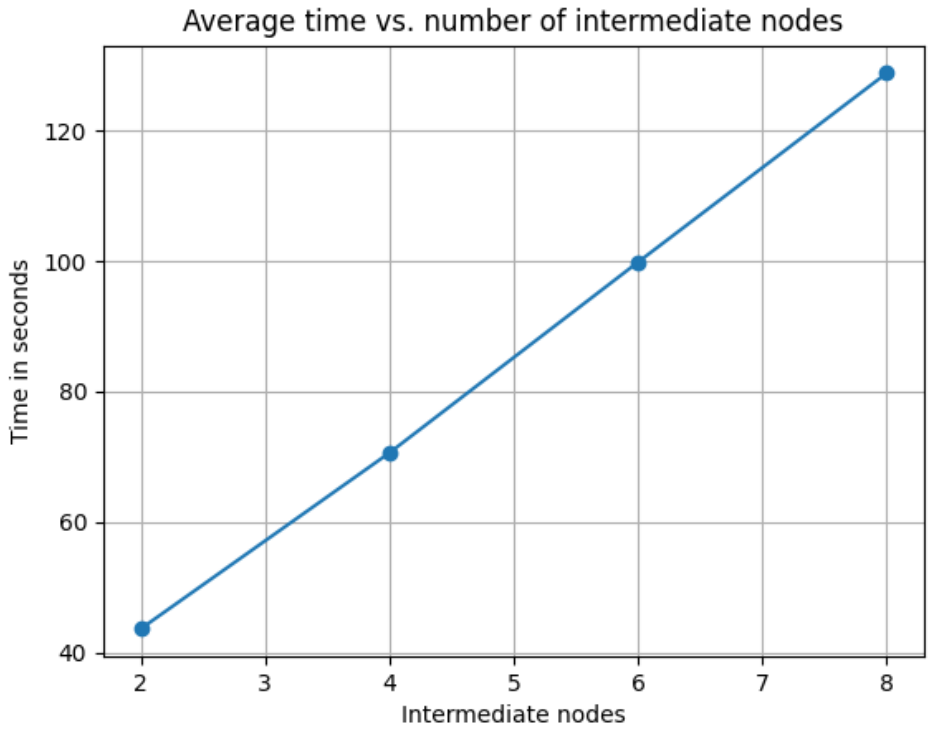

Figure 4.10: INSIM-NS-3D in case Quarter5spot3D execution time

5
Conclusion and Future works

This study focuses on improving the INSIM-FT-3D simulator by reducing its computational cost, minimizing mass inconsistencies, and incorporating compressibility into the second phase of the simulation.

Our initial approach was to develop a numerical solution for the partial differential equation (PDE) associated with the saturation profile using the Finite Difference Method. This research led to the creation of INSIM-NS-3D, a new numerical tool for simulating production in waterflooding reservoirs. This model adapted the computational mesh by including intermediate nodes, which required modifications to the pressure system equations and the descriptions of both the gravitational term and edge transmissibility.

The INSIM-NS-3D model was developed in Python to evaluate potential issues with mass conservation and to compare its performance prediction against commercial simulators. Initial results showed a maximum 2.5% difference in oil production when compared to reference simulations performed with CMG-IMEX. This demonstrates a satisfactory level of agreement between the two models. A key achievement of the new model is the successful incorporation of compressibility into the saturation profile, which was not present in its predecessor, INSIM-FT-3D.

Future work includes determining the optimal number of intermediate nodes per edge, which is currently defined empirically. We also aim to optimize computational performance; efforts are underway to convert the code to the C programming language. The next primary goal is to expand the model to support water-oil-gas simulations.

6
Bibliography

ALGHAREEB, Z.; CHRISTOPHER, J. E. A data-driven proxy model for fast performance prediction of waterflooding in heterogeneous reservoirs. **SPE Reservoir Evaluation & Engineering**, Society of Petroleum Engineers, v. 18, n. 02, p. 234–243, 2015.

BRUNTON, S. L.; KUTZ, J. N. **Data-Driven Science and Engineering: Machine Learning, Dynamical Systems, and Control**. [S.l.]: Cambridge University Press, 2019.

BUCKLEY, S.; LEVERETT, M. Mechanism of fluid displacement in sands. **Transactions of the AIME**, OnePetro, v. 146, n. 01, p. 107–116, 1942.

CHEN, Z. **Reservoir Simulation: Mathematical Techniques in Oil Recovery**. [S.l.]: SIAM, 2007.

COATS K.H., D. J.; HENDERSON, J. The use of an implicit pressure, explicit saturation (impes) scheme in the numerical simulation of waterflooding. **Society of Petroleum Engineers Journal**, Society of Petroleum Engineers, v. 7, n. 03, p. 327–341, 1967. Disponível em: https://doi.org/10.2118/1783-PA.

Computer Modeling Group Ltd. **Computer Modeling Group Simulator Suite**. Calgary, Alberta, Canada, 2024. Version 2024. Disponível em: https://www.cmgsoftware.com/.

DARCY, H. **Les fontaines publiques de la ville de Dijon**. Paris: Dalmont, 1856. In French.

EMERICK, A. A.; REYNOLDS, A. C. Ensemble smoother with multiple data assimilation. **Computers & Geosciences**, v. 55, p. 3–15, 2013.

EYMARD, R.; GALLOUËT, T.; HERBIN, R. Finite volume methods. In: CIARLET, P.; LIONS, J. (Ed.). **Handbook of Numerical Analysis, Volume VII**. [S.l.]: North-Holland, 2000. p. 713–1020.

GRAHAM, R. L. An efficient algorithm for determining the convex hull of a finite planar set. **Information Processing Letters**, v. 1, n. 4, p. 132–133, 1972.

GRAVE, M. et al. A mass conservative insim-ft-3d physics-based data-driven oil-water reservoir simulator. **Geoenergy Science and Engineering**, v. 12, n. 12, p. 213102, 2024. Disponível em: https://www.sciencedirect.com/science/article/abs/pii/S294989102400472X.

GUO, Z.; REYNOLDS, A. C. Insim-ft: A two-dimensional interwell numerical simulation model with front-tracking. **Journal of Computational Physics**, v. 380, p. 143–169, 2019.

KILLOUGH, J. Reservoir simulation with history-dependent relative permeability. **SPE Journal**, Society of Petroleum Engineers, v. 16, n. 01, p. 37–48, 1976.

KISSAS, G. et al. Machine learning in cardiovascular flows modeling: Predicting arterial blood pressure from non-invasive 4d flow mri data using physics-informed neural networks. **Computer Methods in Applied Mechanics and Engineering**, Elsevier, v. 358, p. 112623, 2020.

LEVEQUE, R. J. **Finite Volume Methods for Hyperbolic Problems**. Cambridge: Cambridge University Press, 2002. ISBN 9780521009249.

LI, Y.; ONUR, M. Insim-bhp: A physics-based data-driven reservoir model for history matching and forecasting with bottomhole pressure and production rate data under waterflooding. **Journal of Computational Physics**, v. 473, p. 111714, 2023.

MITCHELL, D. P. Generating antialiased images at low sampling densities. **ACM SIGGRAPH Computer Graphics**, v. 21, n. 4, p. 65–72, 1987.

PEACEMAN, D. W. **Fundamentals of Numerical Reservoir Simulation**. Amsterdam: Elsevier, 1977. ISBN 9780444417471.

PREPARATA, F. P.; SHAMOS, M. I. **Computational Geometry: An Introduction**. New York: Springer-Verlag, 1985.

Python Software Foundation. **Python 3 Reference Manual**. USA, 2024. https://www.python.org/.

RAISSI, M.; PERDIKARIS, P.; KARNIADAKIS, G. E. Physics-informed neural networks: A deep learning framework for solving forward and inverse problems involving nonlinear partial differential equations. **Journal of Computational Physics**, Elsevier, v. 378, p. 686–707, 2019.

RUDY, S. H. et al. Data-driven discovery of partial differential equations. **Science Advances**, American Association for the Advancement of Science, v. 3, n. 4, p. e1602614, 2017.

Schlumberger. **ECLIPSE Industry Reference Reservoir Simulator**. Houston, Texas, USA, 2024. Version 2024. Disponível em: https://www.software.slb.com/products/eclipse.

WILLARD, J. et al. Integrating physics-based modeling with machine learning: A survey. **arXiv preprint arXiv:2003.04919**, 2020.

XIE, Y. et al. Data-driven reduced-order modeling procedure for subsurface flow simulation. **Water Resources Research**, Wiley Online Library, v. 56, n. 4, p. e2019WR026140, 2020.

ZHAO, H. et al. Insim: A data-driven model for history matching and prediction for waterflooding monitoring and management with a field application. In: **Proceedings of the SPE Reservoir Simulation Symposium**. [S.l.: s.n.], 2015. ISBN 978-1-61399-352-1. Paper SPE-173213-MS, Houston, February 23–25,2015.